Structural and kinetic properties of laterally stabilized, oligo(ethylene glycol)-containing alkylthiolates on gold: A modular approach

Ramūnas Valiokas,[a] Mattias Östblom, Fredrik Björefors, and Bo Liedberg[b]
Division of Molecular Physics, Department of Physics, Chemistry, and Biology, Linköping University, SE-581 83 Linköping, Sweden

Jing Shi and Peter Konradsson
Division of Chemistry, Department of Physics, Chemistry and Biology, Linköping University, SE-581 83 Linköping, Sweden

(Received 10 February 2006; accepted 27 February 2006; published 14 April 2006)

The formation of highly ordered self-assembled monolayers (SAMs) on gold from an unusually long and linear compound $HS(CH_2)_{15}CONH(CH_2CH_2O)_6CH_2CONH(CH_2)_{15}CH_3$ is investigated by contact angle goniometry, *ex situ* null ellipsometry, cyclic voltammetry and infrared reflection-absorption spectroscopy. The molecules are found to assemble in an upright position as a complete monolayer within 60 min. The overall structure of the SAM reaches equilibrium within 24 h as evidenced by infrared spectroscopy, although a slight improvement in water contact angles is observed over a period of a few weeks. The resulting SAM is 60 Å thick and it displays an advancing water contact angle of 112° and excellent electrochemical blocking characteristics with typical current densities about 20 times lower as compared to those observed for $HS(CH_2)_{15}CH_3$ SAMs. The dominating crystalline phases of the supporting $HS(CH_2)_{15}$ and terminal $(CH_2)_{15}CH_3$ alkyl portions, as well as the sealed oligo(ethylene glycol) (OEG) "core," appear as unusually sharp features in the infrared spectra at room temperature. For example, the splitting seen for the CH_3 stretching and CH_2 scissoring peaks is normally only observed for conformationally trapped alkylthiolate SAMs at low temperatures and for highly crystalline polymethylenes. Temperature-programmed infrared spectroscopy in ultrahigh vacuum reveals a significantly improved thermal stability of the SAM under investigation, as compared to two analogous OEG derivatives without the extended alkyl chain. Our study points out the advantages of adopting a "modular approach" in designing novel SAM-forming compounds with precisely positioned in plane stabilizing groups. We demonstrate also the potential of using the above set of compounds in the fabrication of "hydrogel-like" arrays with controlled wetting properties for application in the ever-growing fields of protein and cell analysis, as well as for bioanalytical applications. © *2006 American Vacuum Society.* [DOI: 10.1116/1.2188521]

I. INTRODUCTION

Self-assembled monolayers (SAMs) on gold and other metallic surfaces are widely recognized as a convenient platform for the development of novel molecular architectures. The self-assembly process and properties of relatively simple linear bifunctional compounds, e.g., alkylthiols on gold,[1–3] are fairly well understood, and these materials have become of tremendous importance within a broad range of applications, from materials science[4] and nanotechnology[5] to biotechnology[6] and biosensing.[7,8] Naturally, the interest in constructing even more complex supported molecular assemblies using, e.g., oligomeric chains other than polymethylenes, and especially those containing unique structural motifs and hetero groups, has increased significantly over the last few years.

We have undertaken a systematic investigation of structural and kinetic properties of structurally complex monolayers formed by solution self-assembly of oligo(ethylene glycol) (OEG)—containing alkylthiol derivatives. In the biomaterials research community this class of compounds has been used mainly as efficient blockers of the unspecific protein binding to surfaces.[9–11] Further on, poly(ethylene glycol) (PEG) displays interesting physical and structural properties. For example, it exists in a well defined helical crystalline phase in the solid state,[12] and it can be used to form solid, crystalline electrolytes[13] upon coordination with ions such as Li^+. Soft PEG, in the form of a grafted hydrogel,[6] is mainly known for its high exclusion volume. Moreover, it can undergo interesting modifications. In a recent study, Gattas-Asfura *et al.* utilized PEG hydrogels for the immobilization of quantum dots[14] for the development of new sensor materials.

Oligo(ethylene glycol) compounds modified with a thiol anchoring tail are an attractive alternative to PEGs for the generation hydrogel-like coatings on metallic supports. A variety of OEG-containing alkylthiol compounds have been synthesized, assembled and characterized with a broad range of surface sensitive techniques.[9–11,15–24] The vivid discussions in the literature regarding the role of the terminal OEG

[a]Present address: Molecular Compounds Physics Laboratory, Institute of Physics, Savanorių 231, LT-02300 Vilnius, Lithuania.
[b]Author to whom correspondence should be addressed; electronic mail: bol@ifm.liu.se

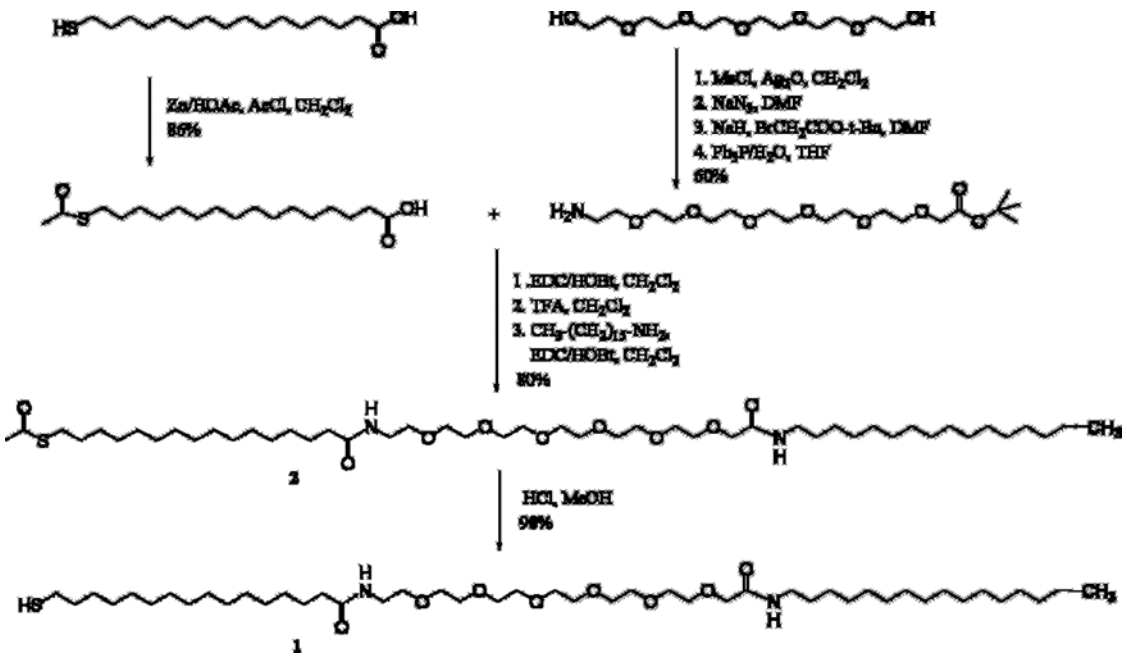

SCHEME 1.

conformation on the protein rejecting properties also encouraged us and others to study protein, plasma and serum adsorption on SAMs with varying alkyl and OEG chain lengths as well as with tail groups.[11,25–27] Furthermore, the choice of linkage groups between the molecular segments offers a strategy to generate OEG SAMs with fine-tuned conformational properties, controlled thermal stability and a unique phase behavior.[23,24]

In the present work we further explore how the choice of structural motifs and tail groups influence the assembly kinetics, equilibrium structure, phase behavior and stability of a novel SAM formed by solution assembly of an extended chain compound $HS(CH_2)_{15}CONH(CH_2CH_2O)_6CH_2CONH(CH_2)_{15}CH_3$ on polycrystalline gold. The results are compared with recent observations obtained for a related system of OEGs,[16,17] where the OEG portion pins directly to gold via the thiol group and forms a crystalline support for a highly ordered outermost layer of the alkyl chains. Our experimental findings are also compared with data obtained for simple alkylthiols and an analogous set of OEG derivatives without the extended alkyl chain, as well as with results from recent theoretical studies[28,29] in order to reveal the influence of the competing intra- and intermolecular interactions on the phase behavior and overall stability of the SAM.

Finally, we demonstrate a potential application of such highly ordered alkyl-terminated OEG SAMs for the fabrication of microarrays based on confined hydrophilic and disordered "hydrogel-like" domains. This type of spatially controlled biointerphase offers a convenient platform for the dissection of individual cells and multi-protein complexes.

II. MATERIALS AND METHODS

A. Synthesis

The synthesis of $HS(CH_2)_{15}CONH(CH_2CH_2O)_nH$, where $n=1,4,6,12$ (EG_n) and $HS(CH_2)_{15}CONH(CH_2CH_2O)_6CH_2CONH(CH_2)_{15}CH_3$ (EG_6C_{16}) was performed as described in detail by Svedhem *et al.*[30] However, by following their reaction protocol, traces of protected compound **2** (in the form of disulphides) were found together with compound **1**. Such disulphides could become a source of defects during the self-assembly process and should therefore be kept at a minimum level. It was therefore decided to slightly modify the reaction conditions during transfer of **2** to **1**, Scheme 1. Acid deprotection was used by dissolving a small amount of **2** (35 mg) in MeOH. The mixture was purged with Ar for 30 minutes. Then, 142 μl of acetyl chloride (AcCl) was carefully dropped into the solution (AcCl reacted with MeOH and formed HCl). The reaction mixture was refluxed under Ar for 60 min to completely deprotect **2**. Finally, the reaction was stopped and repeatedly evaporated with dry toluene followed by additional purification by HPLC.

The structures of deprotected compound **1** and protected compound **2** were obtained by using nuclear magnetic resonance (NMR) (300 MHz) and MALDI-time of flight (TOF) mass Spectrometry. Compound **1**: $HS(CH_2)_{15}CONH(CH_2CH_2O)_6CH_2CONH(CH_2)_{15}CH_3$, ^{1}H NMR ($CDCl_3$) δ 1.25 (br, 50H), 1.52–1.61 (m, 6H), 2.17 (tr, 2H), 2.53 (tr, 2H), 3.43 (tr, 2H), 3.53 (tr, 2H), 3.52–3.66 (m, 20H), 3.98 (s, 2H), 6.29 (s, 1H), 6.99 (s, 1H); ^{13}C NMR ($CDCl_3$) δ 14.2, 22.7, 25.7, 26.9–31.9, 34.0, 36.7, 38.9, 70.0–70.7, 169.7, 173.3. Calcd for $C_{46}H_{92}N_2O_8S$: ($[M+Na]^+$) 855.65 Found: ($[M+Na]^+$) 855.65. Compound **2**: $Ac-S-(CH_2)_{15}CONH$

$(CH_2CH_2O)_6CH_2CONH(CH_2)_{15}CH_3$, ^{1}H NMR ($CDCl_3$) δ 0.85–0.90 (s, 3H), 1.25 (br, 50H), 1.52–1.61 (m, 6H), 2.17 (tr, 2H), 2.32 (s, 3H), 2.85 (tr, 2H), 3.43 (tr, 2H), 3.53 (tr, 2H), 3.52–3.66 (m, 20H), 3.98(s, 2H), 6.29 (s, 1H), 6.99 (s, 1H); ^{13}C NMR ($CDCl_3$) δ 14.1, 22.7, 25.7, 26.9–31.9, 30.6, 36.7, 38.9, 70.0–70.7, 169.7,1 73.3, 196.2. Calcd for $C_{48}H_{94}N_2O_9S$: ($[M+Na]^+$) 897.66 Found: ($[M+Na]^+$) 897.66.

B. Sample preparation

Fresh ethanolic 20μM solutions of the thiol compounds were prepared in plastic beakers from 1 mM stock solutions stored in glass vials at 4 °C. About 2000 Å-thick gold films were electron beam deposited on standard (100)-silicon wafers primed with a 25 Å titanium adhesion layer and used as substrates for the SAMs. The electron beam evaporation of the metals was done in a Balzers UMS 500 P system operating at a base pressure on the low 10^{-9} mbar scale and at an evaporation pressure of about 10^{-7} mbar. A constant evaporation rate of 10 Å/s was used for gold. The resulting polycrystalline gold film was shown to be heavily dominated by a (111) texture.[31] Prior to SAM adsorption, the gold surfaces were cleaned in a 5:1:1 mixture of de-ionized (MilliQ) water, 30% hydrogen peroxide, and 25% ammonia for 5 min at 80 °C, followed by extensive rinsing in de-ionized water. The efficiency of cleaning was always tested before the adsorption of the SAMs. For this purpose, the optical characteristics of a cleaned gold sample were measured using an automatic Rudolph Research AutoEL ellipsometer with a He–Ne laser light source of $\lambda=632.8$ nm, at an angle of incidence of 70°. The rest of the cleaned samples were preconditioned in ethanol and then transferred into the thiol solutions. Before characterization, the samples were rinsed in ethanol, ultrasonicated for 3 minutes, and rinsed again. Finally, they were blown dry in nitrogen gas and immediately analyzed.

Microcontact printing process was carried out as described in detail by Zhou, Valiokas, and Liedberg,[32] except that the PDMS stamp was used without oxygen plasma treatment. The PDMS stamps were inked with the thiols (equimolar amount of EG_1 and EG_4) at a total concentration of 100 μM in ethanol (99.5%, Kemetyl, Haninge, Sweden) for 5 min followed by drying in N_2. The inked stamp was brought in contact with the gold substrate for 3 min. The stamped samples were backfilled in 40 μM EG_6C_{16} solution in ethanol for several hours followed by extensive rinsing and ultrasonication in ethanol to remove low molecular weight PDMS residues and physisorbed thiols.[32]

C. Ellipsometry

For single-wavelength *ex situ* ellipsometry, average values of the refractive index of the clean gold sample were determined prior to incubation. The ellipsometric readings Δ and Ψ of the SAMs were evaluated using a three-layer model "ambient/SAM/gold," assuming an isotropic, transparent ($k=0$) SAM with a refractive index of $n=1.5$. The film thickness was calculated as an average of measurements at three different spots of the sample. For each adsorption time, 4–8 samples were inspected.

D. Contact angle goniometry

Contact angles were measured with a Ramé-Hart NRL 100 goniometer under room conditions, probing the surfaces with fresh de-ionized water from a MilliQ unit. Only one measurement of the advancing and receding contact angle was done per sample, and 4–10 samples were inspected for each adsorption time.

E. Infrared reflection-absorption spectroscopy (IRAS)

The room temperature reflection-absorption (RA) spectra were recorded on a Bruker IFS 66 system, equipped with a grazing angle (85°) infrared reflection accessory and a liquid-nitrogen-cooled mercury cadmium teleuride (MCT) detector. The measurement chamber was continuously purged with nitrogen gas during the measurements. The resolution was 2 cm^{-1} and a three-term Blackmann–Harris apodization function was applied to the interferograms before Fourier transformation. The total acquisition time was around 10 min. A spectrum of a deuterated hexadecanethiolate ($HS(CD_2)_{15}CD_3$) on gold was used as reference.

F. Temperature programmed infrared reflection-absorption spectroscopy

The temperature-programmed measurements were performed in an ultrahigh vacuum (UHV) system which has been described in detail elsewhere.[33] Briefly, a modified Bruker IFS PID 22 spectrometer aligned at a grazing angle of 82° equipped with f/16 transfer optics and a liquid-nitrogen-cooled MCT detector was used to record the temperature-programmed spectra. The spectral resolution was 2 cm^{-1} and 500 interferograms were collected and averaged. The same apodization function was applied to the interferograms as in the case of the room temperature spectra. All spectroscopic data were further analyzed using Bruker OPUS software.

The measurements were performed in a UHV chamber operating at a base pressure of 10^{-10} mbar. The procedure was identical to the one used in our previous work.[23] After setting the temperature of a solid copper sample holder to the desired value (with 5 °C steps), the system was allowed to stabilize for 5 min before collecting the sample spectrum. After the temperature programmed experiment the sample was transferred into a separate preparation chamber for neon ion sputtering. Finally, the background spectrum of a clean gold substrate was recorded.

G. Electrochemistry

An Autolab PGSTAT20 (EcoChemie, Utrecht, the Netherlands) was used for the voltammetric experiments. All experiments were performed in the three-electrode mode using an Ag/AgCl reference electrode and a platinum wire as counter electrode. The SAM coated gold surfaces (working

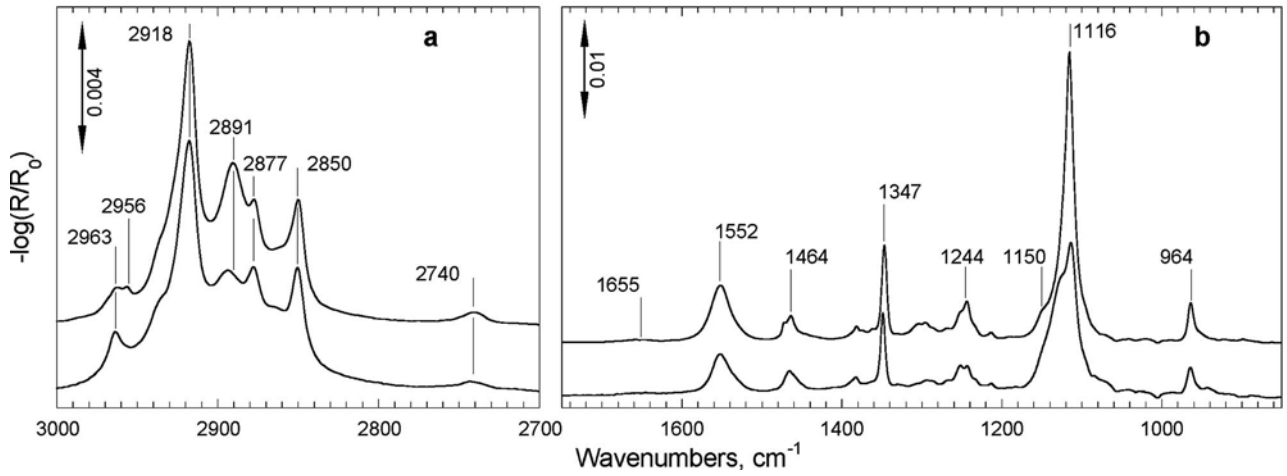

FIG. 1. Room temperature RA spectra of an EG_6C_{16} SAM (adsorption time ten days) (upper curves) and a simulated spectrum obtained by adding spectra of EG_6 and $HS(CH_2)_{15}CH_3$ SAMs, respectively (lower curves). The CH stretching region is depicted in (a) and the fingerprint region in (b).

electrodes) were brought into contact with the test solution via pressfitting to an O-ring in the side of a Kel-F-based electrochemical cell. The exposed area of the electrode was 0.2 cm^2. Cyclic voltammograms were recorded by scanning the potential from +0.60 V (vs Ag/AgCl) to −0.30 V and back, with a scan rate of 10 mV/s. Prior to the scan the electrode was kept at +0.60 V for 10 s. To provide redox species, a 1.0 mM $K_3Fe(III)(CN)_6$ (Merck) solution [also containing 100 mM KNO_3 (Merck) as supporting electrolyte] was used. Voltammograms were also recorded in only the supporting electrolyte solution, i.e., without the redox species.

H. Optical microscopy of microwetting patterns

The condensation pattern of water from the laboratory air to reveal the surface microstructures generated during the printing process was obtained by cooling the micropatterned samples on a Peltier element. The resulting micropattern was visualized using an Olympus BX60 microscope equipped with MPlan and UMPlanFl objectives. An Exwave HAD color video camera was employed to capture the images.

III. RESULTS

A. Equilibrium structural properties

The formation of SAMs of EG_6C_{16} on gold was analyzed by contact angle goniometry, null ellipsometry, cyclic voltammetry and infrared reflection-absorption spectroscopy. It was observed that the measured wettability, ellipsometric thickness and the infrared spectra of the SAM displayed a temporal dependence on the time scale from minutes to weeks. Therefore, we will first comment on the properties of an equilibrated system, i.e., for SAMs prepared by adsorption times not shorter than two weeks. Then we will address the kinetics of the SAM formation process.

The advancing and receding water contact angles measured for EG_6C_{16} SAMs, prepared with an adsorption time of two weeks, displayed high values, $\theta_a = 112°$ and $\theta_r = 108°$, respectively. This is a typical value for a densely packed linear chain alkylthiolate SAM with terminal methyl groups exposed to the ambient.[2] Moreover, the low hysteresis confirms that the SAM is highly oriented, densely packed, chemically and structurally uniform.

The measured ellipsometric thickness was found to be 60.2±0.4 Å, a value comparable to the length of an EG_6C_{16} molecule in an upright position on the surface. Note, that we used a three-layer optical model treating the SAM as a transparent isotropic material with the refractive index $n=1.5$, which certainly is an oversimplification. Nevertheless, the chosen model gives a thickness that is in excellent agreement with values obtained by superimposing the thickness for an oriented SAM of EG_6, 39.8±1.7 Å,[28] and that of a $HS(CH_2)_{15}CH_3$(hereafter SC_{16}) SAM, 19±1 Å[33]

The upper curve in Fig. 1 displays a reflection-absorption (RA) spectrum of an equilibrated EG_6C_{16} SAM. The spectral features in this SAM are compared with those observed in a simulated one (the lower curve), achieved by superimposing separate spectra of SAMs formed by EG_6 and SC_{16}, respectively. In the C–H stretching region [Fig. 1(a)] appears the antisymmetric (d^-) and symmetric (d^+) stretches of the alkyl methylenes at 2918 and 2850 cm^{-1}, respectively.[34] These positions are characteristic for densely packed and highly ordered all trans alkyl chains. Note that the relative intensities of the two alkyl peaks for the EG_6C_{16} SAM are comparable with those of the simulated spectrum. It has to be born in mind, however, that for an exact comparison one needs to account for the intensity contribution from other underlying spectral OEG components in this region. This observation suggests that the order and orientation of the two alkyl layers in the EG_6C_{16} SAM, in fact, resemble those in the analogous SAMs of the EG_6 and SC_{16} compounds, respectively.

The high frequency region also contains strong peaks due to the C–H stretches of the methylenes in the OEG portion of the SAM. Malysheva *et al.* revised recently the infrared spectra of OEGs and we assigned the strongest peak at ~2891 cm^{-1} to the asymmetric C–H stretches of helical

OEG.[35] A drastic increase in the intensity of this peak is observed as compared to the simulated spectrum. This is in line with a better defined helical structure of the OEG motifs and/or a more pronounced orientation of the helical axis parallel to the surface normal.[23,28] The symmetric OEG methylene stretching peak is not as pronounced because of a strong overlap with other bands. Still it can be identified at around 2865 cm^{-1}, as well as a high frequency shoulder on the polymethylene d^- peak near 2937 cm^{-1}. Another characteristic feature of the helical OEG chain is a peak at 2740 cm^{-1}. It is assigned to a combination of CH_2 twisting and bending modes.[12,36]

A remarkable observation in Fig. 1(a) is the appearance of the peaks due to the antisymmetric (r^-) and symmetric (r^+) stretching modes of the terminal methyl group. The latter peak is found in both the simulated and measured EG_6C_{16} SAM spectra at 2877 cm^{-1}. However, the r^- modes of the methyls in the simulated and measured spectra display remarkably different signatures. For long chain alkythiolate SAMs on gold (including SC_{16}) they normally appear as a single feature at around 2963 cm^{-1}.[37] In fact, this peak is a superposition of two antisymmetric modes, a high frequency in-plane component (r_a^-) that dominates this peak, and an out-of-plane component (r_b^-), which appears as a weak shoulder at room temperature. Interestingly, for EG_6C_{16} appears a well-resolved doublet, containing comparable contributions of the r_a^- and r_b^- modes. A similar split of the methyl antisymmetric C–H peak along with a slight increase in the intensity of the symmetric one has been reported for long-chain alkylthiolate SAMs below 200 K.[38,39] The observed splitting of the methyl r^- stretch at room temperature is, however, unusual. This behavior, in general, has been attributed to a reduction of the rotational freedom of the terminal methyl groups, and it is often regarded as an indication of a highly crystalline phase in the SAM. We will discuss this observation in more detail in subsequent section.

The general trend in the low frequency region [Fig. 1(b)] is that the spectrum of EG_6C_{16} SAM exhibits much stronger and sharper features as compared to the simulated one. The region is dominated by sharp peaks at 1347, 1244, 1116 and 964 cm^{-1}, corresponding to CH_2 wagging, twisting, rocking and skeletal stretching modes that are all characteristic for helical OEGs. Recent RA spectra and calculations of EG_6 SAMs[28] suggest that the helical axis of the OEG is portion aligned with a small tilt with respect to the surface normal. For the EG_6C_{16} SAM, all of these peaks are stronger than for EG_6 SAM [which mainly contributes to the simulated spectrum in this region, Fig. 1(b)], and the increase in intensity of the strongest C–O stretching peak at 1116 cm^{-1} is particularly prominent. To reveal the nature of the structural differences between the OEG portions of the EG_6C_{16} and EG_6 SAMs, let us first discuss the various contributions to the appearance of this peak in more detail. The spectrum of the EG_6 SAM contains shoulders at around 1127 and 1150 cm^{-1}. Our previous studies indicate two possible origins of these shoulders. The first one is that they originate from the skeletal modes with a transition dipole moment aligned perpendicular to the helical axis of the OEG chain and that they appear because of a nonzero tilt angle of the helical axis with respect to the surface normal.[12,28,36] The second possibility is that other OEG phases coexist with the helical in the SAM.[20,22] Interestingly, these spectral components, in particular the one at 1127 cm^{-1}, are remarkably reduced for the EG_6C_{16} SAM, and the main feature peaking at 1116 cm^{-1} appears symmetrical, except for a weak high frequency shoulder at 1150 cm^{-1}. Also, the relative intensity and the shape of the 1116 cm^{-1} peak is comparable to that of analogous isostructural SAMs of $HS(EG_6)(CH_2)_mCH_3$ reported by Vanderah and co-workers.[16,20] They attributed the 1116 cm^{-1} peak to an assembly consisting of a single phase of highly ordered helical OEGs. It is therefore reasonable to conclude that these changes in the skeletal modes peak of the EG_6C_{16} SAM, as compared to the EG_6 SAM, are associated with, first of all, an improved crystalline phase of the OEG in terms of the improved helicity, and secondly to better alignment of OEG portion of the SAM along the surface normal.

Another distinctive fingerprint that can be found in the low frequency region is that of the amide groups. The two amide moieties along the chain of EG_6C_{16} are expected to stabilize the overall structure of the SAM by forming two layers of lateral hydrogen bonds.[23,24] The appearance of oriented lateral hydrogen bonds between the amides can be detected as frequency shifts and relative intensity changes of the so-called amide I and amide II modes. Indeed, in the spectrum of the EG_6C_{16} SAM, the amide I peak (C═O stretch) is nearly absent (likewise in the case of EG_6), and only a broad, ill-defined, feature is seen at around 1656 cm^{-1}. This observation strongly supports a preferential orientation of the C═O groups parallel to the surface. At the same time, the amide II peak of EG_6C_{16} at 1552 cm^{-1} (a combined C–N stretching and C–N–H bending mode) appears stronger by ~70% as compared to the EG_6 SAM. This is consistent with two parallel layers of hydrogen bonded amide moieties in the EG_6C_{16} SAM. Ideally one would expect a 100% increase in the amide II peak intensity if exactly the same structure of the hydrogen-bonded amides appears in the upper and lower layers. Apparently, there is a slight difference in their orientation with respect to the surface normal. Nevertheless, the strong anisotropy of the two amide peaks confirms the high degree of ordering in the EG_6C_{16} assembly.

The last observation that is worth noting in the low frequency region is the structure of the CH_2 scissoring modes peak. For the EG_6 SAM, this peak appears as a broad feature centered around 1466 cm^{-1} [Fig. 1(b)], and it contains contributions both from the alkyl and OEG portions of the SAM.[40,24] However, the upper spectrum shown in Fig. 1(b) reveals a sharp split of the scissoring peak into two major components 1472 and 1464 cm^{-1}. This is again similar to the behavior of long chain alkylthiolate SAMs at low temperatures,[38] and correlates well to a highly ordered structure.

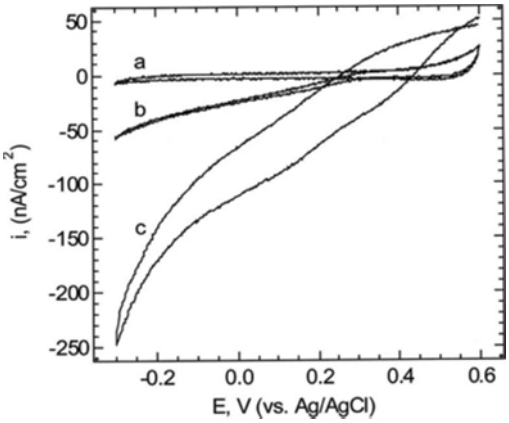

FIG. 2. Cyclic voltammograms for the EG_6C_{16} SAM (after 24 h adsorption) in (a) only the supporting electrolyte (100 mM KNO_3), and (b) 1.0 mM $K_3Fe(III)(CN)_6$ (100 mM KNO_3 as supporting electrolyte). In (c) is the voltammogram for a EG_6 SAM in 1.0 mM $K_3Fe(III)(CN)_6$ (100 mM KNO_3 as supporting electrolyte). The scan rate was 10 mV/s.

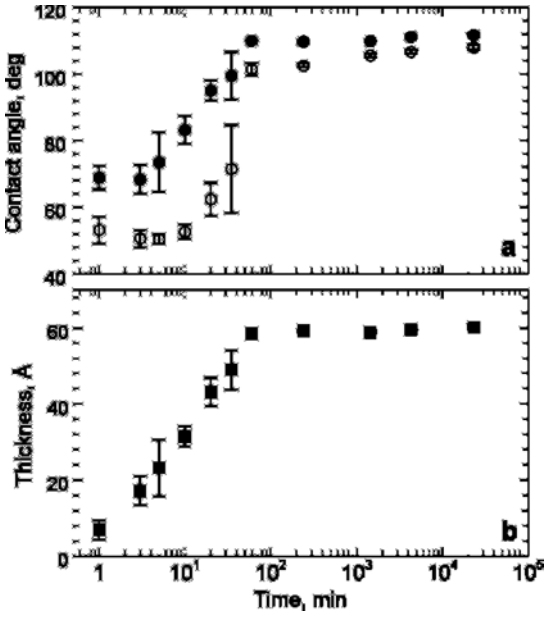

FIG. 3. Adsorption kinetics of the EG_6C_{16} SAM from an ethanolic solution: (a) advancing (filled symbols) and receding (open symbols) water contact angles; (b) SAM thickness determined by *ex situ* null ellipsometry. The error bars represent the standard deviation.

B. Blocking characteristics

Based on the suppression of faradic reactions, cyclic voltammetry (CV) gives information on the blocking characteristics of molecular films. This technique is also useful for qualitative evaluation of the molecular ordering of a SAM.[41] Thus, for the present EG_6C_{16} monolayers, CV was used to study the ordering and blocking properties, and for comparison with the analogous EG_6 SAMs without the extra $C_{15}CH_3$ layer. The very low current density and the shape of voltammogram b in Fig. 2 confirm that the EG_6C_{16} thiols form well ordered SAMs, and that they almost completely block faradic reactions. At, for example, −0.3 V, the current density is ~ -60 nA/cm^2, which is about 20 times lower compared to what we normally obtain for a SC_{16} SAM under the same experimental conditions. The latter SAM is usually considered sufficiently thick and well organized to demonstrate good blocking characteristics. The voltammogram for EG_6C_{16} recorded in only the supporting electrolyte is shown in Fig. 2(a). Except for the length of the molecules, the enhanced intermolecular interactions in combination with the hydrophobic property of the external alkyl layer are two of the main explanations for the excellent blocking properties obtained with the EG_6C_{16} SAMs.

Voltammogram (b) in Fig. 2 also demonstrates that the low current still present for reduction of $Fe(III)(CN)_6^{3-}$ starts to increase close to the formal potential for the redox couple ($E^{\circ\prime} \approx 0.2$ V vs Ag/AgCl), which likely means that small amounts of naked gold are exposed on the sample. The overall current density is, however, too low to originate from a substantial number of ordering defects and/or pinholes in the monolayer, or from accidentally formed defects at the O-ring seal. The majority of the faradic reactions most likely take place at gold exposed due to packing disorders at imperfections in the gold substrate.[42] However, considering the length of the molecules, i.e., ~60 Å, even gold at grain boundaries and step sites can be covered to a high extent. Although the shape of the voltammograms obtained for the EG_6 SAMs [Fig. 2(c)] were basically the same as those from EG_6C_{16}, the current density was found to be about four times larger. Given the fact that the EG_6 molecules are ~20 Å shorter and lack a second stabilizing amide layer, they do not cover gold at grain boundaries and step sites to the same extent. The outer layer of the EG_6 SAMs is also more hydrophilic, which facilitates penetration of redox species.

C. Self-assembly kinetics

Figure 3 represents the results from *ex situ* measurements of the EG_6C_{16} SAM adsorption kinetics using contact angle goniometry and null ellipsometry. The advancing and receding contact angles [Fig. 3(a)] observed during the first 60 min display high hysteresis (~20–30°) suggesting that the layers formed are inhomogeneous. A continuous increase of the thickness [Fig. 3(b)] occurs in parallel with a constant increase in the hydrophobicity of the SAM, and on going from the 40th to the 60th minute, the hysteresis drops remarkably. After this point, the SAM thickness changes marginally. However, some minor rearrangements of the outermost layers of the SAM are revealed by the contact angle measurements obtained for this second phase. The advancing contact angle increases by a few degrees and levels off at 112° during the next several days of adsorption, and the hysteresis continues to decrease to about 4°.

In order to relate the above observations to the structural events in the EG_6C_{16} SAM, we employed in parallel *ex situ* IRAS measurements. Unfortunately, this approach was found to be problematic because of significant batch-to-batch variations of the absolute peak intensities during the initial phase of the adsorption process. For example, the peak intensity of the 1116 cm^{-1} band measured after 5 min adsorption in one

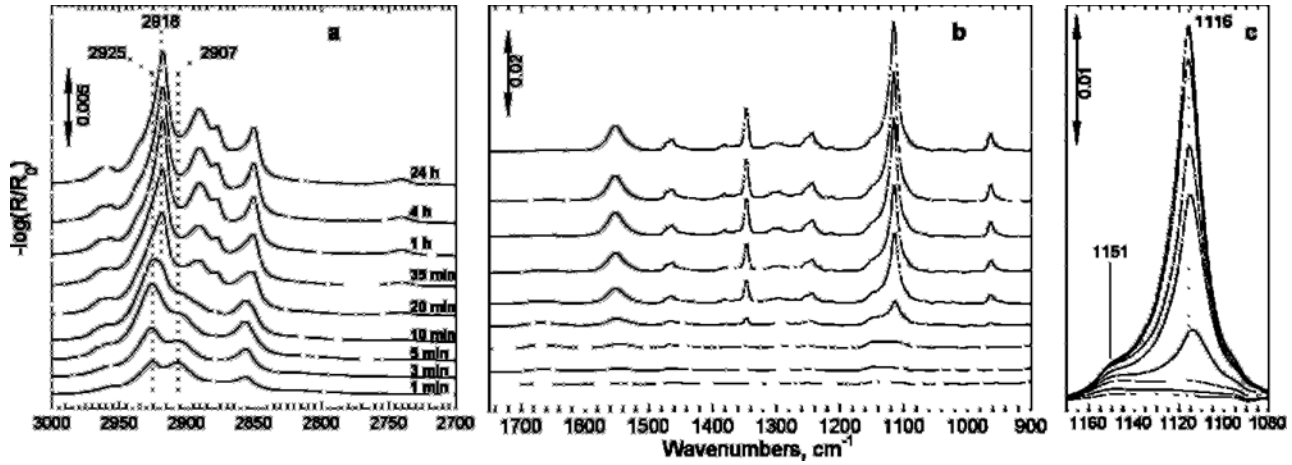

FIG. 4. *Ex situ* infrared RA spectra showing the adsorption kinetics. Representative spectra in the CH stretching (a), fingerprint (b) regions. Panel (c) shows the skeletal COC region.

batch could be higher than that after 20 minutes in the other. This observation is perhaps not that surprising considering the inherent conformational flexibility of the EG_6C_{16} molecule. Thus, quantitative analysis of the adsorption kinetics by IRAS would need a large number of experiments, which is not absolutely necessary in this case, keeping in mind a good reliability of the ellipsometric results. On the other hand, the main time-dependent conformational and/or orientation changes were always observed to occur in the same sequence. Therefore, in Figs. 4(a) and 4(b), we show the evolution of the infrared RA spectra, which are obtained by combining results from several measurement series, and they can be used for a qualitative description of the critical events occurring during the self-assembly of the EG_6C_{16} molecules.

The C–H stretching region, Fig. 4(a), confirms that a significant amount of the molecules appear on the gold surface already after 1 min, Fig. 4(a). The two methylene stretches d^- and d^+ appear at 2925 and 2855 cm^{-1}, respectively, and indicate the presence of disordered "liquid-like" alkyl chains.[43] Interestingly, a strong peak that normally does not appear in spectra of alkanethiolate SAMs is found at 2907 cm^{-1}. In previous studies by Yamamoto *et al.*, this peak was assigned to "softening" of methylene CH vibrations upon direct interaction with a metal surface[32,44,45] A comparison of the relative peak intensities in the CH region, Fig. 4(a), with the above cited spectroscopic investigations of long chain alkane films on gold suggests that the amount of the material adsorbed during the first minutes corresponds to a fraction of a monolayer of EG_6C_{16} molecules with disordered alkyl chains in a flat-on arrangement. The increasing thickness of the adsorbed layer manifests itself by the increasing d^- and d^+ peak intensities on going from 1 to 10 min. On going from 10 to 20 min, a pronounced shift of the d^- peak from 2925 to 2918 cm^{-1} is observed, a consequence of an alkyl phase transition from a gauche rich to all trans conformation. Moreover, the alkyl phase transition occurs in parallel with the formation of a helical OEG [Fig. 4(b)]. Subsequent spectral changes, i.e., the growth of the helical C–O peak at 1116 cm^{-1} as well as the related ones at 2891 cm^{-1} [Fig. 4(a)], 1464, 1347, 1244, 964 cm^{-1} [Fig. 4(b)], are associated with an increase in the amount of the helical phase and alignment of the helical axes along the surface normal. Note that a relatively high order is confirmed already between 20 and 35 min of the adsorption. The d^- peak at 2918 cm^{-1} sharpens and the broad feature due to the methyl r^- vibrations splits into the two components during this step. A clear saturation of the intensity growth at 1116 cm^{-1} is observed within the first 2 h, indicating that most of the structural rearrangements of the OEG portion of the SAM are completed [Fig. 4(c)]. This is also seen as a stabilization of the other helical peaks in the CH and fingerprint regions [Figs. 4(a) and 4(b)]. For example, the integrated intensity of the isolated helical peak at 1347 cm^{-1} is

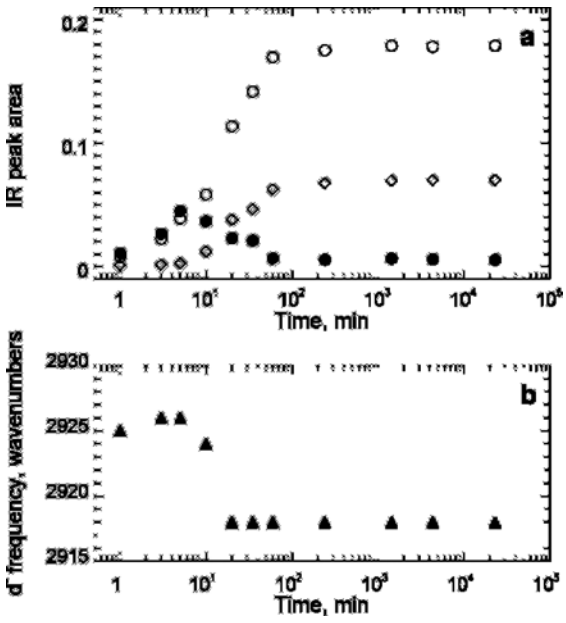

FIG. 5. (a) Changes in integrated intensities of the peaks assigned to the EG_6 wagging mode (open circles), amide I (filled circles) and amide II (diamonds) modes. (b) Changes of alkyl d^- frequency (filled triangles).

plotted in Fig. 5 (open circles) to demonstrate this behavior. The amide I and II bands also vary in relative intensity during the assembly phase. As the helical structure and the orientation of the OEG portion improves (Fig. 5, open circles), a simultaneous drop in the amide I intensity is noted (Fig. 5, filled circles). In parallel, the amide II peak (diamonds) gains intensity. Also, the alkyl segments of the constituent molecules undergo a pronounced disorder to order transition seen in the IR spectrum as a downward shift of the d^- peak from 2925 to 2918 cm^{-1}. The alkyl phase ordering seems to occur somewhat faster than the corresponding rearrangements of the OEG and the amide portions. Taking together, the above IRAS observations suggest that the main structural rearrangements of the SAM are accomplished within 24 h of the adsorption process, since the RA spectra recorded after one day are virtually identical in terms of the finest spectral details.

D. Thermal behavior

Temperature-programmed IRAS (TP-IRAS) is a powerful method to explore the influence of various inter- and intramolecular interactions on the thermal stability and phase behavior of SAMs. We have employed this technique to verify that the additional layers of amide bonds and alkyl chains delay the temperature driven phase transitions of the "sealed" OEG phase and, in a broader sense, how they contribute to the overall stability of the EG_6C_{16} SAM. Therefore, we compare this system with two analogous SAMs, EG_6 and EG_{12}, that have no extended alkyl chain. The EG_6 SAM has been extensively examined in our earlier studies.[23,46] Moreover, the assembly of the EG_{12} compound has been described in previous work by Svedhem *et al.*[30] Figure 6 shows the evolution of the OEG peaks in the region of the skeletal COC stretching modes with substrate temperature, between (T_o, T_f) °C. These peaks are most informative in terms of the structural changes occurring during the phase transitions. The results for the EG_6 SAM, Fig. 6(c), are taken from earlier studies by Valiokas *et al.*[23,46] For this SAM, a unique phase transition was found to occur in the OEG portion of the SAM at around 60 °C, which we interpreted as the transition from the dominating helix to all trans conformations. In the COC region, this process can be observed as a gradual decrease of the main peak component due to the helical crystalline phase at 1114 cm^{-1} upon stepwise heating, followed by a relatively fast increase in intensity at 1144 cm^{-1} when the temperature approaches the phase transition temperature at ~60 °C. This new peak reaches maximum intensity at ~75 °C and is related to the formation of all trans OEG conformers in the SAM.[23,46]

A similar phase behavior is also found for the EG_{12} SAM, Fig. 6(d). The main COC stretching peak appears initially at 1120 cm^{-1}. It is sharp and strong, a consequence of the formation of a crystalline-like phase of helical EG_{12} tails. Moreover, peak integration in the COC region reveals that the ratio I_{EG12}/I_{EG6} is about 1.8, an observation in satisfactory agreement with a value of 2 which is the expected ratio because of the twofold increase in chain length. For this SAM,

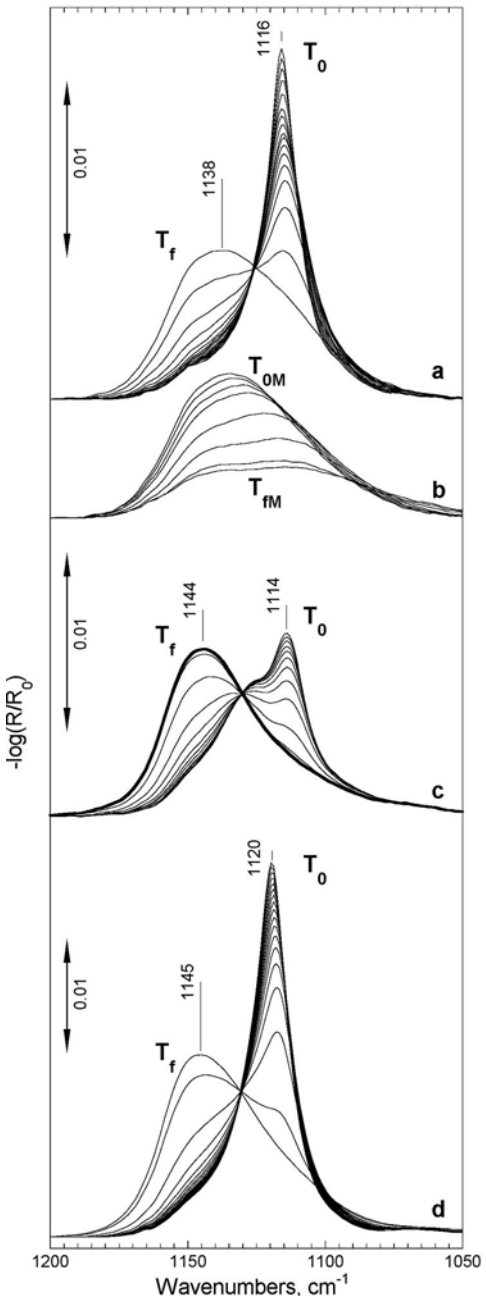

FIG. 6. Temperature-induced phase transitions of the OEG portions of the SAMs under investigation, seen in the spectral region of the skeletal COC modes (measured by TP-IRAS in ultrahigh vacuum): (a) EG_6C_{16} $(T_o, T_f) = (20, 140)$ °C; (b) EG_6C_{16} $(T_{oM}, T_{fM}) = (145, 180)$ °C; (c) EG_6 $(T_o, T_f) = (20, 75)$ °C; and (d) EG_{12} $(T_o, T_f) = (20, 105)$ °C. The temperature ramping was performed in steps of 5 °C. Panel (a) shows a transition from helical to amorphous OEG on going from 20 to 140 °C, and panel (b) illustrates the subsequent melting and decomposition of the same SAM occurring between 145 and 180 °C. Panel (c) (taken from the previous study by Valiokas *et al.* (see Ref. 23), and panel (d) show the helical to all trans phase transitions on going from 20 to 75 °C and 20 to 105 °C, respectively.

the phase transition is shifted to higher temperatures and occurs at 95 °C, and the intensity gain of a new peak formed at 1145 cm^{-1} levels off at ~105 °C. The shape and position the COC peak is similar to that observed in the RA spectrum for the EG_6 SAM at 75 °C and our previous experimental and

theoretical studies[23,28] suggest that the all trans phase dominates in the EG_{12} SAM at high temperatures.

Contrary to the OEG-terminated analogs, the helical crystalline OEG phase in the EG_6C_{16} SAM turns, most likely, into an amorphous-like state on going from 20 to 140 °C, Fig. 6(a). This is evidenced by an appearance of a broad peak centered at 1138 cm^{-1}, a feature that is known to indicate the presence of the conformational disorder along the OEG chain.[23,24] On the other hand, even at 140 °C a shoulder is observed at close to 1116 cm^{-1}, and it suggests that some helical conformers are still present in the SAM. The second major difference in phase properties of EG_6C_{16} and the other two SAMs under investigation is that the helix to amorphous-like phase transition occurs at a surprisingly high temperature: it is completed at ~140 °C. Above this temperature, the intensity of the skeletal COC peak broadens and decreases in intensity, Fig. 6(b), indicating a gradual loss of the orientation, an overall disordering of the SAM (a sort of melting transition), and ultimately decomposition and concomitant reduction of coverage.

To learn more about the correlation of the phase transitions in the OEG and alkyl portions of the EG_6C_{16} SAM, one can follow the thermal evolution of the alkyl d^- frequency [Fig. 7(a)], the integrated intensities of the amide I [Fig. 7(b)] and wagging mode peak [Fig. 7(c)]. The latter follows the behavior of the helical peaks at 1244, 1116, and 964 cm^{-1}, but it is taken here for convenience to compare the stability of the OEG phase in the three different SAM systems.[23]

Figure. 7(a) shows a plot of the alkyl d^- frequency versus substrate temperature for the EG_6C_{16} SAM. A frequency shift from 2918 to 2920 cm^{-1} is seen upon increasing the substrate temperature to 125 °C and it corresponds to a slight increase in the amount of gauche defects along the alkyl chain. This moderate disordering can also be seen as a gradual lowering of the d^- and d^+ peak intensities (data not shown), most probably, due to a gradual untilting of the alkyl chains, as has been observed for linear long-chain alkylthiolates.[43] We always found a similar d^- and d^+ intensity loss upon heating for the OEG-terminated alkylthiolate SAMs, including EG_6 and EG_{12}. The second process that occurs in parallel with the upward shift of the d^- frequency is the rapid transformation of the sharp r^- doublet near 2960 cm^{-1} into a single broad peak dominated by the r_a^- mode (see Ref. 61). The overall disordering effect is also observed as the disappearance of the 1473 cm^{-1} component of the methyl scissoring modes.

The number of defects in OEG portion is also expected to increase upon raising the temperature to ~125°. For example, a lowering of the helical peak intensity [Fig. 7(c)] is always seen in the RA spectra. We would like to stress, however, that the observed changes in the structure of the alkyl and OEG portions do not seem to affect the network of the lateral hydrogen bonds. The amide II peak, which is sensitive to variations in the hydrogen bonding pattern, does not change (see Ref. 61), and the intensity of the amide I remains close to zero [Fig. 7(b)] within the temperature range 20–125°.

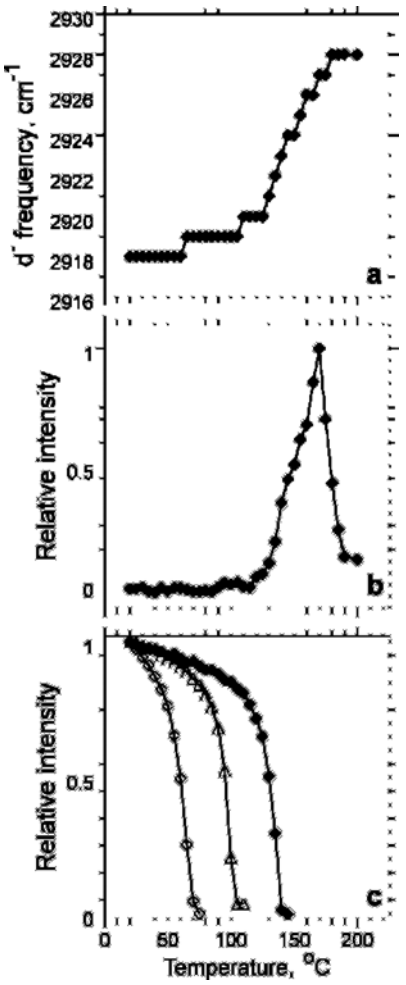

FIG. 7. Frequency shift of the alkyl d^- mode (a) and changes of the normalized integrated intensity of the amide I peak (b) from the same series of TP-IRAS measurement on EG_6C_{16} as shown in Fig. 5(a). Panel (c) shows temperature dependence of normalized integrated intensities of the peak assigned to the wagging mode at 1349 cm^{-1} for EG_6 (open diamonds), EG_{12} (triangles) and EG_6C_{16} (filled diamonds) SAMs. Based on this analysis, the phase transition temperatures can be identified at 60, 95 and 135 °C, respectively.

An abrupt shift of the d^- frequency starts at around 125° [Fig. 7(a)]. In parallel, we observe the onset of the intensity gain of the alkyl C–H peaks (see Ref. 61). This behavior of the alkyl peaks can be interpreted as a loss of the orientation of the polymethylene chains and an overall increase in disorder of the SAM.[23,24,43] The loss of the OEG wagging peak intensity also accelerates, and it is reduced to 50% of its initial intensity at ~130° [Fig. 7(c)]. This point, i.e., at 50% intensity loss, was in our previous study identified as the helical-to-amorphous/all trans phase transition temperature.[23] Note that the phase transitions for the EG_6 and EG_{12} SAMs occur at around 60 and 95°, respectively [Fig. 7(c)]. Close to the OEG phase transition temperature the structural rearrangements take place in the whole EG_6C_{16} SAM. This is evidenced, for example, by the amide I intensity increase

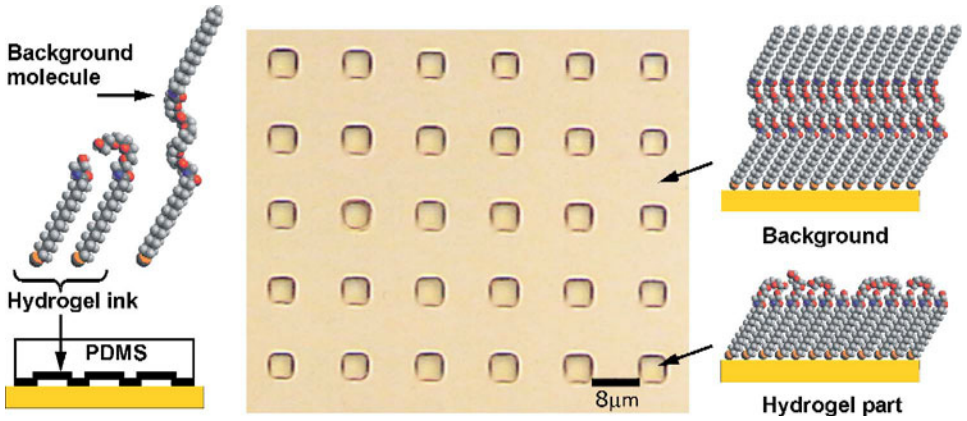

FIG. 8. Schematic illustration of a hydrogel array composed of 4×4 μm^2 spots generated via positive microcontact printing of a mixture of OEG-terminated alkylthiols (EG_1 and EG_4) followed by backfilling with the EG_6C_{16} molecule. The microwetting image is obtained with an Olympus BX60 microscope by placing the sample on a Peltier element held at a temperature below the dew point (about 16 °C). Note that the lateral dimensions of the space filling models are not to scale.

[Fig. 7(b)], suggesting the loss of the orientation of the C═O groups. Moreover, the rupture of the lateral hydrogen bonding network is also confirmed by the frequency shift of the amide II band (see Ref. 61).

The increase in disordering of the EG_6C_{16} SAM is progressing until the intensities of the amide I band [Fig. 7(b)] and those of the alkyl C–H peaks (not shown) reach their maximal values at around 170 °C. Heating of the sample beyond this point causes decomposition of the SAM as all the spectral peaks start to loose intensities [see, for example, the C═O peak, Fig. 7(b), and the region of the OEG skeletal modes, Fig. 6(b)].

We have previously tested the reversibility of these temperature-driven processes for different OEG-terminated alkylthiolate SAMs.[23] Cooling down of the sample from a temperature just above the phase transition temperature back to 20 °C revealed a nearly full recovery of the helical OEG phase. Therefore, in the present study we also tested the reversibility for the EG_6C_{16} SAM, by gradually heating the sample to 140 °C and then cooling it down to 20 °C (see Ref. 61). After such a heating cycle no structural changes were found in the alkyl portions of the SAM, as evidenced by the infrared RA spectra. However, the OEG peaks revealed irreversible changes, i.e., the OEG portion of the annealed SAM consisted of a mixture of helical, all trans and amorphous phases.

E. Microwetting of hydrogel-like SAM patterns

The structural order and dense packing of the terminal alkyl chains of the EG_6C_{16} compound and the conformational flexibility of the EG_n tails[23,47] turn them into attractive candidates for microfabrication of surface patterns consisting of alternating hydrophobic, hydrophilic and/or order-disorder domains. Such micropatterns are interesting, for example, in the field of supported lipid membranes[48] and for the confinement and subsequent analysis of complex protein architectures or individual cells.[7] For this purpose, EG_6C_{16} was used as a backfilling molecule to confine hydrogel-like domains consisting of mixed SAMs of compounds EG_1 and EG_4 (molar ratio 1:1) microcontact printed on gold. We have previously shown that ordered hydrophilic micropatterns can be obtained via microcontact printing OEG-terminated thiols with hydrophilic (treated with oxygen plasma) PDMS stamps.[32] In this proof of principle experiment, however, hydrophobic (nontreated) stamps were used. Backfilling with EG_6C_{16} for several hours, after EG_n printing, revealed a sharp water condensation pattern on the gold surface, Fig. 8, even when the feature (square) size was as small as 4×4 μm^2. The microscopic water droplets condensed exclusively within the OEG-terminated domains, whereas the EG_6C_{16} SAM provided an efficient nonwetting background. This observation is in agreement with the large difference in advancing water contact angles measured for the EG_6C_{16} and mixed EG_1 and EG_4 SAMs assembled from solution, 112° and 38°, respectively. Note that the created array elements consist of hydrogel-like (disordered) OEG tails for the EG_1 and EG_4 compounds.

IV. DISCUSSION

The employed set of surface analytical techniques shows that the investigated EG_6C_{16} compound forms a highly ordered and stable SAM on gold. The unusually sharp features in the CH and fingerprint regions of the RA spectra and the improved thermal stability of this SAM are governed by favorable intra- and intermolecular interactions. However, an exact account of their relative contributions to the ultimate equilibrium structure of the EG_6C_{16} SAM is beyond the scope of the present study. Although IRAS provides crucial information about the orientation and conformation of the molecular constituents, we are still lacking information about the positional order and island/domain formation. Such information requires extensive analyses with diffraction and scanning probe techniques.

The multi-step kinetics involved in the EG_6C_{16} SAM formation is known from previous studies of long-chain alkylthiolates on gold (reviewed by Schwartz[49]), and our contact

angle, ellipsometric and IRAS results clearly allow us to discriminate between two major phases of the SAM formation process. Our data also reveal certain differences in the self-assembly mechanism as compared to that reported for "simple" alkylthiolates (compounds without complex tail groups). The coverage and conformational order changes continuously during the initial, relatively fast, phase. This phase is virtually accomplished within ~60 min a process which is slower by one order of magnitude than that seen for simple alkylthiolate SAMs prepared under similar conditions.[2] Further on, we observe a second, much slower phase, which involves conformational and tail group rearrangements, while the overall SAM thickness and surface coverage remain constant. Thus, in terms of the monolayer growth the self-assembly kinetics of the EG_6C_{16} SAM can be regarded as one-step process that is followed by a much slower rearrangement process leading to a highly oriented and densely packed assembly. The equilibrium SAM structure, as revealed by IRAS, is reached within 24 h (Figs. 4 and 5). Also cyclic voltammetry shows that the EG_6C_{16} SAM efficiently blocks the electrode reactions after 24 h, Fig. 2. Only small changes in orientation are taking place upon increasing the adsorption time, most likely, in the terminal portion of the molecules as evidenced by slightly increasing contact angles (hydrophobicity) and decreasing contact angle hysteresis [Fig. 3(a)].

Despite of the structural complexity of the EG_6C_{16} molecule, it does not follow the behavior reported for SAMs generated from polymeric "PEG-like" thiol compounds.[50,51] The adsorption kinetics for these PEG-like thiol compounds deviated remarkably from a Langmuir model, and displayed an extended period (~10 min) within which hardly no adsorption appears to take place. Contrary, the formation of the EG_6C_{16} SAM is reminiscent of Langmuir kinetics, which also was found to satisfactory describe the formation of "simple" alkylthiolate SAM studied under similar experimental conditions.[52] Moreover, the correlation between the onset of the increase in the advancing contact angle [Fig. 3(a)] and the appearance of helical OEG peaks in the RA spectra [Fig. 4] cannot rule out the possibility that the layer growth occurs via formation of islands containing EG_6C_{16} molecules adopting the helical OEG conformation. Therefore, a more detailed topographic analysis, similar to the SPM study carried out by Rundqvist, Hoh, and Haviland,[51] would be necessary to improve the understanding of the mechanism(s) behind the EG_6C_{16} SAM formation.

Based on our IRAS results, we also propose that the RA spectra of the equilibrated EG_6C_{16} SAMs, surprisingly though, contain a number of features that, so far, have only been observed for highly crystalline SAM of long chain alkylthiolates on gold at low temperatures,[38,39] or in highly crystalline polymethylenes.[53] In particular, we would like to draw the attention to the splitting of the methyl C–H antisymmetric stretching and methylene scissoring peaks, a behavior, which in earlier studies has been attributed to the formation of a bimolecular monoclinic phase, where the all trans C–C backbone in neighboring alkyls is rotated 90° with respect to one another.[37,38,53] At higher temperatures is the splitting masked by the rapidly increasing population of gauche defects in the methylenes near the terminal methyl group leading to a coalescence of the r^- and r^+ modes. Applying the same method of reasoning for our EG_6C_{16} SAM would mean that we are dealing with a virtually defect-free crystalline phase of the terminal alkyl chains reminiscent of a bimolecular monoclinic phase. Thus, the template of supporting alkyls (SC_{15}), highly crystalline OEG helices and aligned amide dipoles seems to facilitate the terminal alkyl chains to accommodate a structure that is close to that found in polymethylene crystals.[53] On the other hand, a certain degree of conformational flexibility in the OEG portion could also help optimizing the interaction between the neighboring alkyl tails. Such flexibility might in our case occur because the terminal alkyls do not have to follow exactly the $(\sqrt{3} \times \sqrt{3})R30^\circ$ template defined by the sulfur atoms pinned to the Au(111) substrate. The lateral hydrogen bonds could be another important factor contributing to the formation of the bimolecular monoclinic phase in the upper layer of the alkyls. This way of reasoning is supported by the fact that analogous SAMs[16,20] composed of long-chain alkyls attached to a thiol modified OEG tail (HS-OEG-alkyl), displayed no splitting of the methyl C–H antisymmetric stretching and methylene scissoring peaks. It should be stressed, however, that Vanderah *et al.*[16,20] employed a slightly different strategy to synthesize the compounds, where an ether group was used instead of an amide group to link the OEG and alkyl portions of the molecule.

The improvement of the thermal stability of the EG_6C_{16} SAM compared to SAM of simple alkylthiolates and EG_n:s, is most likely due to favorable intermolecular interactions occurring between preferentially aligned amides and densely packed terminal alkyl chains. The importance of laterally interacting amides on the thermal stability of SAMs was addressed in a recent study where TPD data from SAMs prepared from a $HS(CH_2)_{18}OH$-thiol was compared with data obtained for an equally long EG_1 SAM (a compound where a CH_2 group is replaced by an amide group).[24] The present study undoubtedly suggests that the EG_6C_{16} SAM is far more stable than long-chain alkylthiolate SAMs. For example, the disordering process, seen as the onset of an abrupt upward shift of the d^- frequency, starts at 125 °C for the EG_6C_{16} SAM as compared to 77 °C in the case of the latter system.[43] Interestingly, in the above-cited study the critical temperature was found to be independent of the alkyl chain length and the type of the terminal group. In the case of the EG_6C_{16} SAM, the total van der Waals contribution of the terminal $C_{15}CH_3$ chain can be estimated to fall in the range 96–108 kJ/mol.[54,55] This interaction together with the lateral hydrogen bonds formed by the second layer of amide groups ~20–25 kJ/mol,[56,57] creates a substantial energy barrier that has to be overcome during the phase transition. As a result, the intermolecular interactions increase the phase transition temperature for the OEG portion of the SAM roughly by a factor of 2 as compared to the EG_6 SAM, Fig. 7(c).

Finally, we demonstrate also herein a possible future application of the EG_6C_{16} SAM, where the terminal alkyls act as barriers separating hydrogel-like domains generated by microcontact printing using EG_n compounds as ink. Previous studies have shown that densely packed alkyl monolayers can provide a support for self-assembled hybrid bilayers, a model system that constitutes a platform for cell membrane mimetics.[48,58,59] Furthermore, the OEG-terminated hydrogel-like domains, when functionalized with specific anchoring groups, can be used to properly immobilize functionally active proteins[7,8,60] Also, the hydrophobic barriers are of high importance in the fabrication of protein arrays via piezodispensing.[32] Our study suggests that the EG_6C_{16} SAMs could be utilized as such hydrophobic barriers in the fabrication of protein and lipid membrane arrays. The superior thermal stability of the SAM could be advantageous in various micro- and nanofabrication processes of biochips, e.g., UV photolithography, laser ablation, etc. Also, the excellent blocking characteristics measured under electrolyte conditions indicated that the EG_6C_{16} SAM is stable in aqueous environments. Moreover, interesting hydrophilic-hydrophobic, ordered-disordered phases could be generated and patterned by mixing EG_6C_{16} with shorter compounds such as EG_6. Likely, such mixed SAMs would display more complex behavior in terms of their interaction with water and with biological molecules such as lipids.

Modern nanolithographic methods can be used to generate hydrophilic-hydrophobic arrays similar to the one shown in Fig. 8 with element sizes at a scale of tens of nanometers. Possibly, biomimetic cell membranes like liposomes and bilayers could be supported in these arrays by the nanoscopic domains of the hydrophobic EG_6C_{16} SAMs. Thus, the ability of EG_6C_{16} to form well-defined, robust and relatively thick SAMs provides an attractive strategy for the surface micro- and nanopatterning and for bioanalytical applications. Specific applications of the EG_6C_{16} SAMs will reported on elsewhere.

V. CONCLUSIONS

We have investigated the self-assembly kinetics and conformation of highly ordered EG_6C_{16}SAMs on gold, an extended-chain derivative of previously investigated OEG-terminated alkylthiol compounds. Although the rate of adsorption for EG_6C_{16} compound is much slower than for long-chain alkylthiolates, the kinetics is still best described by a simple Langmuir model. Infrared RA spectra in the alkyl stretching and bending regions of nearly equilibrated SAMs display features that are reminiscent of a bimolecular monoclinic phase found for long-chain alkylthiolates at low temperatures and for crystalline polymethylenes, and the OEG portion of the SAMs is crystalline with the helical axis aligned preferentially along surface normal. Also, cyclic voltammetry of nearly equilibrated SAMs displays excellent blocking characteristics. However, a fully equilibrated SAM structure is achieved only after two weeks of adsorption. The resulting SAM is 60 Å thick, it is highly hydrophobic (an advancing water contact angle of 112°) and it displays low contact angle hysteresis.

Further on, we also investigated the thermal stability of the EG_6C_{16} SAM by TP-IRAS in ultrahigh vacuum. The EG_6C_{16} SAM displays a significant delay of both the alkyl chain disordering and OEG phase transitions as compared to other alkylthiolate and OEG SAM systems. The irreversible helical to amorphous transition of the OEG portion occurs at a very high temperature, ~135 °C. Note that the corresponding helical to all trans transition in the EG_6 SAM occurs at ~60 °C. Further heat treatment of the EG_6C_{16} SAM above 135 °C leads to melting, decomposition and desorption of the SAM building blocks.

Moreover, our study shows that microcontact printed hydrogels separated by protruding alkyl domains of EG_6C_{16} provides new means to fine tune the physico-chemical properties of solid surfaces, e.g., for microarray applications.

ACKNOWLEDGMENTS

This project was a part of the Biomimetic Materials Science program funded by the Swedish Foundation for Strategic Research (SSF) and the Swedish Research Council (VR). F.B. acknowledges the Carl Trygger Foundation. R.V. acknowledges the Swedish Institute (SI) for the support through the Visby program. The authors are thankful to Dr. Yuryi Klymenko and Dr. Lyuba Malysheva for valuable discussions regarding the interpretation of the spectroscopic results. Dr. Šarūnas Petronis is acknowledged for the fabrication of masters used in the microcontact printing experiments.

[1]M. D. Porter, T. B. Bright, D. L. Allara, and C. E. D. Chidsey, J. Am. Chem. Soc. **109**, 3559 (1987).
[2]C. D. Bain, E. B. Troughton, Y. T. Tao, J. Evall, G. M. Whitesides, and R. G. Nuzzo, J. Am. Chem. Soc. **111**, 321 (1989).
[3]F. Schreiber, Prog. Surf. Sci. **65**, 151 (2000).
[4]Y. N. Xia and G. M. Whitesides, Annu. Rev. Mater. Sci. **28**, 153 (1998).
[5]J. C. Love, L. A. Estroff, J. K. Kriebel, R. G. Nuzzo, and G. M. Whitesides, Chem. Rev. (Washington, D.C.) **105**, 1103 (2005).
[6]W. Senaratne, L. Andruzzi, and C. K. Ober, Biomacromolecules **6**, 2427 (2005).
[7]E. Ostuni, L. Yan, and G. M. Whitesides, Colloids Surf., B **15**, 3 (1999).
[8]S. Svedhem, L. Ohberg, S. Borrelli, R. Valiokas, M. Andersson, S. Oscarson, S. C. T. Svensson, B. Liedberg, and P. Konradsson, Langmuir **18**, 2848 (2002).
[9]C. Pale-Grosdemange, E. S. Simon, K. L. Prime, and G. M. Whitesides, J. Am. Chem. Soc. **113**, 12 (1991).
[10]K. L. Prime and G. M. Whitesides, J. Am. Chem. Soc. **115**, 10714 (1993).
[11]P. Harder, M. Grunze, R. Dahint, G. M. Whitesides, and P. E. Laibinis, J. Phys. Chem. B **102**, 426 (1998).
[12]T. Miyazawa, K. Fukushima, and Y. J. Ideguchi, J. Chem. Phys. **37**, 2764 (1962).
[13]G. S. MacGlashan, Y. G. Andreev, and P. G. Bruce, Nature (London) **398**, 792 (1999).
[14]K. M. Gattas-Asfura, Y. J. Zheng, M. Micic, M. J. Snedaker, X. J. Ji, G. D. Sui, J. Orbulescu, F. M. Andreopoulos, S. M. Pham, C. M. Wang, and R. Leblanc, J. Phys. Chem. B **107**, 10464 (2003).
[15]K. L. Prime and G. M. Whitesides, Science **252**, 1164 (1991).
[16]D. J. Vanderah, C. W. Meuse, V. Silin, and A. L. Plant, Langmuir **14**, 6916 (1998).
[17]D. J. Vanderah, C. P. Pham, S. K. Springer, V. Silin, and C. W. Meuse, Langmuir **16**, 6527 (2000).

[18]D. J. Vanderah, G. Valincius, and C. W. Meuse, Langmuir **18**, 4674 (2002).
[19]D. J. Vanderah, J. Arsenault, H. La, R. S. Gates, V. Silin, C. W. Meuse, and G. Valincius, Langmuir **19**, 3752 (2003).
[20]D. J. Vanderah, R. S. Gates, V. Silin, D. N. Zeiger, J. T. Woodward, C. W. Meuse, G. Valincius, and B. Nickel, Langmuir **19**, 2612 (2003).
[21]D. J. Vanderah, H. L. La, J. Naff, V. Silin, and K. A. Rubinson, J. Am. Chem. Soc. **126**, 13639 (2004).
[22]D. J. Vanderah, T. Parr, V. Silin, C. W. Meuse, R. S. Gates, H. Y. La, and G. Valincius, Langmuir **20**, 1311 (2004).
[23]R. Valiokas, S. Svedhem, M. Ostblom, S. C. T. Svensson, and B. Liedberg, J. Phys. Chem. B **105**, 5459 (2001).
[24]R. Valiokas, M. Ostblom, S. Svedhem, S. C. T. Svensson, and B. Liedberg, J. Phys. Chem. B **106**, 10401 (2002).
[25]J. Benesch, S. Svedhem, S. C. T. Svensson, R. Valiokas, B. Liedberg, and P. Tengvall, J. Biomater. Sci., Polym. Ed. **12**, 581 (2001).
[26]D. Schwendel, R. Dahint, S. Herrwerth, M. Schloerholz, W. Eck, and M. Grunze, Langmuir **17**, 5717 (2001).
[27]S. Herrwerth, W. Eck, S. Reinhardt, and M. Grunze, J. Am. Chem. Soc. **125**, 9359 (2003).
[28]L. Malysheva, A. Onipko, R. Valiokas, and B. Liedberg, J. Phys. Chem. A **109**, 7788 (2005).
[29]L. Malysheva, A. Onipko, R. Valiokas, and B. Liedberg, Appl. Surf. Sci. **246**, 372 (2005).
[30]S. Svedhem, C. A. Hollander, J. Shi, P. Konradsson, B. Liedberg, and S. C. T. Svensson, J. Org. Chem. **66**, 4494 (2001).
[31]L. Bertilsson and B. Liedberg, Langmuir **9**, 141 (1993).
[32]Y. Zhou, R. Valiokas, and B. Liedberg, Langmuir **20**, 6206 (2004).
[33]I. Engquist, I. Lundstrom, and B. Liedberg, J. Phys. Chem. **99**, 12257 (1995).
[34]A. N. Parikh and D. L. Allara, J. Chem. Phys. **96**, 927 (1992).
[35]L. Malysheva, Y. Klymenko, A. Onipko, R. Valiokas, and B. Liedberg, Chem. Phys. Lett. **370**, 451 (2003).
[36]L. Malysheva, A. Onipko, R. Valiokas, and B. Liedberg, J. Phys. Chem. B **109**, 13221 (2005).
[37]P. E. Laibinis, G. M. Whitesides, D. L. Allara, Y. T. Tao, A. N. Parikh, and R. G. Nuzzo, J. Am. Chem. Soc. **113**, 7152 (1991).
[38]R. G. Nuzzo, E. M. Korenic, and L. H. Dubois, J. Chem. Phys. **93**, 767 (1990).
[39]I. Engquist and B. Liedberg, J. Phys. Chem. **100**, 20089 (1996).
[40]R. G. Nuzzo, L. H. Dubois, and D. L. Allara, J. Am. Chem. Soc. **112**, 558 (1990).
[41]H. O. Finklea, in *Electroanalytical Chemistry: A Series of Advances* (1996), Vol. 19, pp. 109–335.
[42]S. E. Creager, L. A. Hockett, and G. K. Rowe, Langmuir **8**, 854 (1992).
[43]F. Bensebaa, T. H. Ellis, A. Badia, and R. B. Lennox, J. Vac. Sci. Technol. A **13**, 1331 (1995).
[44]M. Yamamoto, Y. Sakurai, Y. Hosoi, H. Ishii, K. Kajikawa, Y. Ouchi, and K. Seki, J. Phys. Chem. B **104**, 7363 (2000).
[45]M. Yamamoto, Y. Sakurai, Y. Hosoi, H. Ishii, K. Kajikawa, Y. Ouchi, and K. Seki, J. Phys. Chem. B **104**, 7370 (2000).
[46]R. Valiokas, M. Ostblom, S. Svedhem, S. C. T. Svensson, and B. Liedberg, J. Phys. Chem. B **104**, 7565 (2000).
[47]A. J. Pertsin, M. Grunze, and I. A. Garbuzova, J. Phys. Chem. B **102**, 4918 (1998).
[48]J. Lahiri, P. Kalal, A. G. Frutos, S. T. Jonas, and R. Schaeffler, Langmuir **16**, 7805 (2000).
[49]D. K. Schwartz, Annu. Rev. Phys. Chem. **52**, 107 (2001).
[50]S. Tokumitsu, A. Liebich, S. Herrwerth, W. Eck, M. Himmelhaus, and M. Grunze, Langmuir **18**, 8862 (2002).
[51]J. Rundqvist, J. H. Hoh, and D. B. Haviland, Langmuir **21**, 2981 (2005).
[52]O. Dannenberger, M. Buck, and M. Grunze, J. Phys. Chem. B **103**, 2202 (1999).
[53]R. G. Snyder, M. Maroncelli, H. L. Strauss, and V. M. Hallmark, J. Phys. Chem. **90**, 5623 (1986).
[54]R. G. Nuzzo, B. R. Zegarski, and L. H. Dubois, J. Am. Chem. Soc. **109**, 733 (1987).
[55]D. J. Lavrich, S. M. Wetterer, S. L. Bernasek, and G. Scoles, J. Phys. Chem. B **102**, 3456 (1998).
[56]A. J. Doig and D. H. Williams, J. Am. Chem. Soc. **114**, 338 (1992).
[57]Y. K. Kang, J. Phys. Chem. B **104**, 8321 (2000).
[58]A. L. Plant, Langmuir **9**, 2764 (1993).
[59]S. A. Glazier, D. J. Vanderah, A. L. Plant, H. Bayley, G. Valincius, and J. J. Kasianowicz, Langmuir **16**, 10428 (2000).
[60]A. Tinazli, J. L. Tang, R. Valiokas, S. Picuric, S. Lata, J. Piehler, B. Liedberg, and R. Tampe, Chemistry-a European Journal **11**, 5249 (2005).
[61]See EPAPS Document No. E-BJIOBN-1-008601 for five figures with captions. This document can be reached via a direct link in the online article's HTML reference section or via the EPAPS homepage (http://www.aip.org/pubservs/epaps.html).